HAL
open science

Stress Gradient Determination in Anti-Corrosion Multilayer Coating

Pierre-Antoine Dubos, Quentin Hatte, Pascal Casari, Mireille Richard-Plouet, Pierre-Yves Jouan, Samuel Branchu, Nadia Guitter

To cite this version:

Pierre-Antoine Dubos, Quentin Hatte, Pascal Casari, Mireille Richard-Plouet, Pierre-Yves Jouan, et al.. Stress Gradient Determination in Anti-Corrosion Multilayer Coating. Materials Science Forum, 2018, 941, pp.1632-1638. 10.4028/www.scientific.net/MSF.941.1632 . hal-03408646

HAL Id: hal-03408646

https://hal.science/hal-03408646v1

Submitted on 14 Mar 2023

HAL is a multi-disciplinary open access archive for the deposit and dissemination of scientific research documents, whether they are published or not. The documents may come from teaching and research institutions in France or abroad, or from public or private research centers.

L'archive ouverte pluridisciplinaire **HAL**, est destinée au dépôt et à la diffusion de documents scientifiques de niveau recherche, publiés ou non, émanant des établissements d'enseignement et de recherche français ou étrangers, des laboratoires publics ou privés.

Stress gradient determination in anti-corrosion multilayer coating

DUBOS Pierre-Antoine[1, a *], HATTE Quentin[1, 2, b], CASARI Pascal[1, c], RICHARD-PLOUET Mireille[3, d], JOUAN Pierre-Yves[3, e], BRANCHU Samuel[1, f] and GUITTER Nadia[4, g]

[1]Université de Nantes, GeM, Institut de Recherche en Génie Civil et Mécanique, 58 rue Michel Ange, BP420, 44600 Saint-Nazaire, France

[2]Institut de Recherche Technologique Jules Verne, IRT, Chemin du Chaffault, 44340 Bouguenais, France

[3]Université de Nantes, IMN, Institut des Matériaux Jean Rouxel, 2 rue de la Houssinière, Nantes, France

[4]Socomore, avenue Paul Duplaix, ZI Du Prat, 56000 Vannes, France

[a]pierre-antoine.dubos@univ-nantes.fr, [b]quentin.hatte@irt-jules-verne.fr, [c]pascal.casari@univ-nantes.fr, [d]Mireille.Richard@cnrs-imn.fr, [e]Pierre-Yves.Jouan@cnrs-imn.fr, [f]samuel.branchu@univ-nantes.fr, [g]n.guitter@socomore.com

Keywords: Stress, Coating, Thin film, Sol-gel, PVD, Multilayer.

Abstract. To reduce maintenance and to increase the corrosion protection and lifetime of maritime structures while complying with environmental standards, multilayer coatings are applied to protect steel sections. A new generation of hybrid sol-gel and/or HiPIMS Ni-based thin films appear to constitute an efficient pre-treatment before the anti-corrosion paint application. However, increasing the number of coatings and associated interfaces may lead to coating failure due to stresses induced by the different deposition processes. Therefore developing smart models to assess the stress distribution along these multilayers appears of significant importance. The well-known Stoney formula cannot be used for multilayers and owing to the large dimensions of the object to be protected. To assess an easily measurable curvature after deposition, thin steel sheets are used but do not respect any more the Stoney hypotheses. So we set up an analytical thermo-elasto-plastic model to evaluate the stresses induced by depositions in each layer. This model is based on the various thermal expansion coefficients of every coat. After extrapolation along the complete thickness, combining sol-gel and PVD deposition smoothens the stress difference between steel and paint. The shear stresses at interface seems thus to be reduced. The evolution of the stress difference between layers with the imposed deflection can predict the mechanical strength and the interface failure. In order to evaluate the quality of the model, *in-situ* four-point bending in SEM was performed to study of the adhesion between the various layers. The results deduced from the model are in good agreement with SEM images.

Introduction

In recent years, in order to follow environmental standards, a new generation of anticorrosive coatings appeared [1]. Nevertheless, these coatings should also be competitive in terms of corrosion protection and longer in terms of lifetime. A possible improvement seems to perform a combination of chemical and physical surface treatment before application of anticorrosive paint on a metallic part. The implementation of these treatments involves residual stress development [2] which could be harmful, in particular for the adhesion between paint and metallic part. The aim of this work is to suggest implementing a multilayer coating combining Physical Vapor Deposition (PVD) and sol-gel process before painting, briefly detailed due to the project highly confidential in a first part. This study deals with the characterization of these multilayer coatings and especially with the residual stress induced by the deposition processes. In the first part, the used analytical thermo-elasto-plastic model will be described to, in a second part, compare three strategies of coatings and purpose a tool

of choice from simple measurements. The last part will be devoted to the establishment of an original method of adhesion characterization for a multilayer system by *in-situ* four-point bending in SEM.

Experimental work and model details

Deposition process and material features. In this study several samples made of materials and thin films deposited by various processes were investigated. The approach was to leverage existing sol-gel and PVD technologies in High-Power Impulse Magnetron Sputtering (HiPIMS) mode to provide adhesion and corrosion protection. These two techniques were used as surface treatment before epoxy barrier painting. Substrates were cut from a low carbon cold-rolled steel sheet with a thickness of 0.02 mm. Length and width were set to 50 and 5 mm to get a beam. This geometry is chosen to obtain a measurable curvature due to stress development. An extrapolation to a massive part with the analytical model will allow determining induced stress in this kind of structures. Prior to surface treatment steel was cleaned with, a phosphoric acid solution before sol-gel process, or thanks to an ultrasonic bath of ethanol before PVD. Sol-gel process is an ambient chemical route to synthesize a hybrid organic-inorganic material. The coating is based on metal oxide and organic coupling agents to enhance adhesion between substrate and paint [3-5]. It consists of a dilute aqueous zirconium and functionalized silicon alkoxide solution sprayed on the steel substrate. The film was dried under ambient laboratory conditions before paint application. Nickel/Nickel oxide thin films were grown in a HiPIMS system [6-8]. The PVD coating is a 2 layers film: one dense nickel layer to minimizing the oxidation of iron by preventing the diffusion of corrosive species and one nickel oxide layer as an electronic insulating barrier. The nickel layer was deposited for 30 minutes prior to the nickel oxide layer. This one was deposited for 30 minutes with an oxygen flow rate of 5 sccm that increased the working pressure from 0.4 Pa to 0.6 Pa. The coating was cooled under ambient laboratory conditions for at least one hour before paint application.

Table 1. Material parameters for substrate and for each layer. $^{(*)}$ Commonly used values.

			S355 Steel	Ni	NiO	Sol-gel	Paint
Thickness	t	[µm]	30 (or 1 cm)	3	1	2	450
Young Modulus	E	[GPa]	182	33.5	31.2	4.7	8.8
Elastic strain	ε_{el}	[µε]	1300	200 [9]	2100 [12]	?	3200
Poisson ratio	ν	[-]	$0.3^{(*)}$	0.3 [10]	0.3 [10]	0.5 [14]	$0.5^{(*)}$
TEC	α	[1/K]	$1.1\text{x}10^{-5(*)}$	$1.3\text{x}10^{-5}$ [11]	$1.7\text{x}10^{-5}$ [13]	$1.1\text{x}10^{-4}$ [14]	$1.1\text{x}10^{-4(*)}$
H-S parameters	A	[-]	250	775 [9]	15746 [12]	?	313
	B	[-]	265	2.5 [9]	0.19 [12]	?	0.72
	n	[-]	0.88	0.8 [9]	1.1 [12]	?	0.69

Table 1 summarizes the parameters used to calculate the stress gradient. Thickness measurements are performed by Scanning Electron Microscopy along the deposition axis. Young modulus is determined by nano-indentation following Oliver and Pharr methodology [15]. Tensile tests are performed on the substrate and on a dog-bone shape molded sample of paint. Stress-strain curves are fitted with a classical elasto-plastic Hockett-Sherby (H-S) behavior law (Eq. 4). For the other layers, the same law was extracted with literature data. No results on sol-gel were found and mechanical tests turned out to be very complex and hence, as a first approximation, the H-S parameters are considered to be similar to those of paint. The radius curvature induced by the deposition process was measured by image analysis on stereo-micrographs. The last part of experimental characterizations consists in *in-situ* four-point bending in SEM. Several incremental displacements are performed with a relaxation (around 10 N) in order to take an image. The region

of interest is the most strained at the middle of both fulcrums. For these tests, steel substrate thickness is 4 mm based on the device geometry.

Stress in multilayer coatings: analytical model. The analytical model is based on the model for predicting thermal residual stresses in multilayer coating systems introduced by Zhang et al. [16]. This model involves digitally applying a temperature difference which causes, due to the various TEC, a stress gradient linked to a strain gradient across the thicknesses of layers. This model takes into account separately the deformation due to the linear thermal expansion ε^T and the deformation due to the induced bending ε^K. To assess to the first one, the equilibrium condition causes the summation of the in-plane forces in the global system should be zero. For the second, the bending moment should be balanced by the in-plane forces and the sum of the moment with respect to the bending axis should be zero. With those considerations, the curvature K which is the inverse of the radius of curvature ρ (experimentally achievable) can be expressed by Eq. 1. In this equation n layers of coating with individual thickness t_i will be considered on a substrate with a thickness t_s. The position of the interface between the substrate and the first layer is defined by the altitude $z=0$ and the corresponding value $h=t_s$. The subscripts i, s and k are respectively relative to the considered layer, the substrate and the influence of the other layer on the considered layer. $\Delta\alpha$ is the difference between α_s and α_i. Three situations of deposition are investigated: the first one is only paint on steel, the second one is an addition of a sol-gel layer between steel and paint and the last one is a multilayer made up of Ni and NiO deposit by PVD, before spraying sol-gel and then the last layer is the paint.

$$K_i = -\frac{\left\{3\sum_{i=1}^{n}\frac{E_i}{1-\nu_i}t_i(2h_{i-1}+t_i)\left[\frac{E_s}{1-\nu_s}t_s\Delta\alpha_i\Delta T+\sum_{k=1}^{n}\frac{E_k}{1-\nu_k}t_k(\alpha_k-\alpha_i)\Delta T\right]+3\frac{E_s}{1-\nu_s}t_s\sum_{i=1}^{n}\frac{E_i}{1-\nu_i}t_it_s\Delta\alpha_i\Delta T\right\}}{\left\{2\frac{E_s}{1-\nu_s}t_s\left[3\delta^2-3\delta t_s+t_s^2\right]+\sum_{i=1}^{n}2\frac{E_i}{1-\nu_i}t_i\left[3h_{i-1}^2+2h_{i-1}t_i+t_i^2+3\delta^2+3\delta(2h_{i-1}+t_i)\right]\right\}\left(\sum_{i=1}^{n}\frac{E_i}{1-\nu_i}t_i+\frac{E_s}{1-\nu_s}t_s\right)} \quad (1)$$

where δ is the distance from the bending axis to the interface between the substrate and the first layer and can be obtained by Eq. (2):

$$\delta = \frac{\frac{E_s}{1-\nu_s}t_s^2-\sum_{i=1}^{n}\frac{E_i}{1-\nu_i}t_i(2h_{i-1}+t_i)}{2\left(\frac{E_s}{1-\nu_s}+\sum_{i=1}^{n}\frac{E_i}{1-\nu_i}t_i\right)} \quad (2)$$

Residual stresses can be expressed by Eq. (3) which is separated in two equations for layers and for substrate. In each equation the first part is relative to the elastic deformation (if $\varepsilon<\varepsilon_{el}$) and the second part with the H-S coefficients is relative to the plastic strain (if $\varepsilon>\varepsilon_{el}$). $K(z+\delta)$ corresponds to the deformation due to the induced bending ε^K. Deformations due to the thermal expansion ε^T are detailed by Eq. (4).

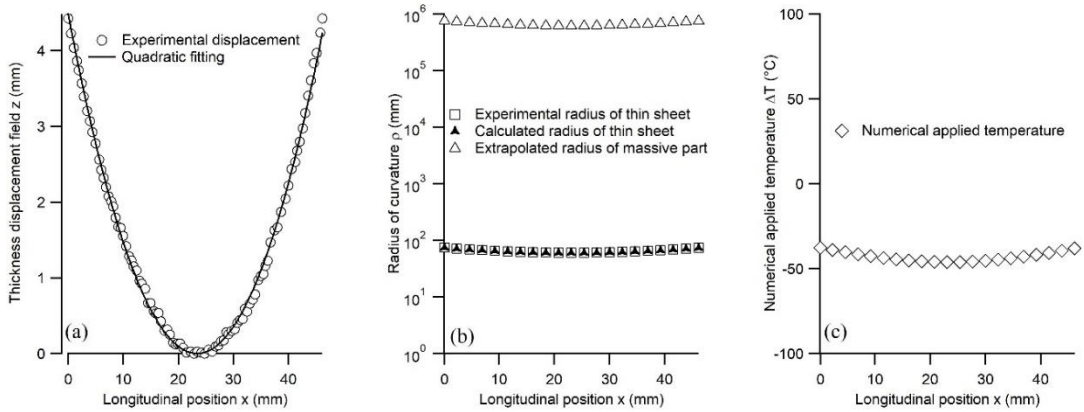

Fig. 1. Example of experimental z displacement field (a) and its corresponding radius of curvature in comparison with the simulation (b). Numerical applied temperature to reproduce experimental results (c).

$$\begin{cases}\sigma_i(z) = E_i\left(\varepsilon_i^T + K(z+\delta)\right) + Aexp\left[1 - B\left(\varepsilon_i^T + K(z+\delta) - \varepsilon_i^{el}\right)^n\right] & for\ 0 \le z \le h_i \\ \sigma_s(z) = E_s\left(\varepsilon_s^T + K(z+\delta)\right) + Aexp\left[1 - B\left(\varepsilon_s^T + K(z+\delta) - \varepsilon_s^{el}\right)^n\right] & for\ -t_s \le z \le 0\end{cases} \quad (3)$$

$$\varepsilon_i^T = \frac{\frac{E_s}{1-\nu_s}t_s\Delta\alpha\Delta T + \sum_{k=1}^{n}\frac{E_k}{1-\nu_k}t_k(\alpha_k+\alpha_i)\Delta T}{\sum_{i=1}^{n}\frac{E_i}{1-\nu_i}t_i + \frac{E_s}{1-\nu_s}t_s} \quad and \quad \varepsilon_s^T = -\frac{\sum_{i=1}^{n}\frac{E_i}{1-\nu_i}t_i\Delta\alpha\Delta T}{\sum_{i=1}^{n}\frac{E_i}{1-\nu_i}t_i + \frac{E_s}{1-\nu_s}t_s} \quad (4)$$

Fig. 1 depicts the principle of this model. In a first time, image analysis enables to extract the field of *z* displacement along the sample length (a). Experimental points are fitted with a polynomial function requisite to calculate the experimental radius of curvature (b). Then a solver is used to minimize the difference between experimental and calculated (following Eq. 1) curvature. This computation is performed to apply a numerical temperature difference ($\Delta T<0$ to have $\rho>0$ and inversely), shown in Fig. 1 (c). A good agreement between experimental and analytical radius shows a good reliability of the solver. An example of an extrapolation to a massive substrate (1 cm thickness) approves that the radius has not been reportable.

Results and discussion

Induced processing deposition stress. Once the macroscopic curvature is numerically reproduced, residual stresses are estimated by means of Eq. (3), first for thin steel sheet and finally for a massive steel piece.

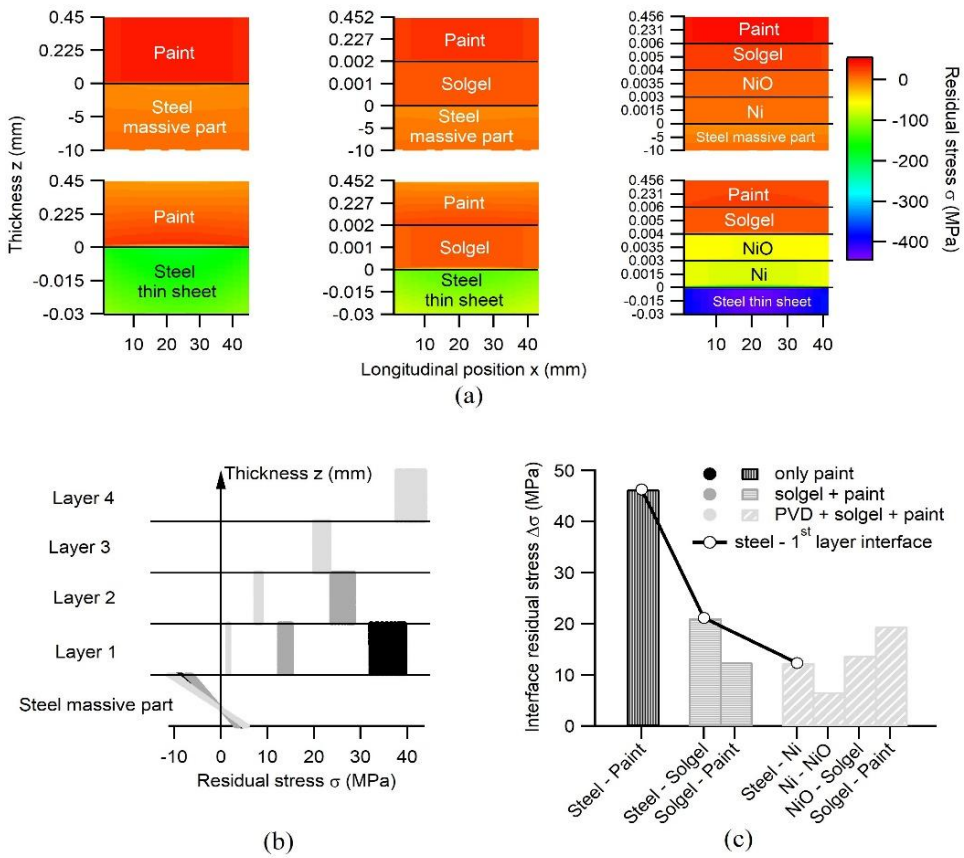

Fig. 2. Stress gradient maps for thin sheet (experimental) (a) and for massive part (extrapolated) (a) and (b). Interface residual stress between each layer for the massive steel part (c)

The three cases previously described are studied and their associated residual stressed are mapped in Fig. 2 (a). The stress determination is performed along the deposition axis *z* with variable steps due to several layers having different thicknesses. The floating step is chosen to keep a number of points equal to fifty in each layer. Fig. 2 (a) and (b) show clearly that an addition of transitional layers between steel and paint softens the sharp stress transition. The combined addition

of PVD layers and sol-gel layer is even more favorable than sol-gel deposition only. However, if a sol-gel layer is sprayed between steel and paint, the paint layer seems less stressed. The adhesion between layers can be quantified by the interface residual stress $\Delta\sigma$ which is the absolute stress difference between two layers at the interface. This value is comparable with a shear stress. Fig. 2 (c) shows that the interface stress between steel and the first layer has more than halved by the PVD layers addition in comparison with the system without transition layer. As a result of the good adhesion between Ni and steel, if paint is degraded, the structure will always be protected against corrosion by the PVD layers in agreement with previous results [17, 18]. Moreover, the combination PVD and sol-gel as transition layers, overall reduced interface stresses, providing a better mechanical behavior.

Prediction of the interface failure, in-situ four-point bending in SEM. *In-situ* four-point bending in SEM is performed on rectangular band with dimensions (50x10x4 mm^3), shown in Fig. 3(b). The used loading cell bears a maximum at 5 kN. Several incremental displacements are performed on the three configurations. For each displacement, an image taken with SEM allows checking the layers and interfaces integrity. A calibration links the imposed displacement and the radius of curvature. In a second step, the previous model is used without the thermal contribution in order to estimate internal stresses in each layer. Fig. 3 (a) is a stress map identified between the fulcrums for various displacements on a sol-gel and paint system. In the top part, the progress of plasticity is plotted. In this figure, it is clearly visible that the most stressed interface lies between steel and sol-gel. This result gives a good prediction on the interface failure and is in agreement with the observed delamination on the micrograph (c).

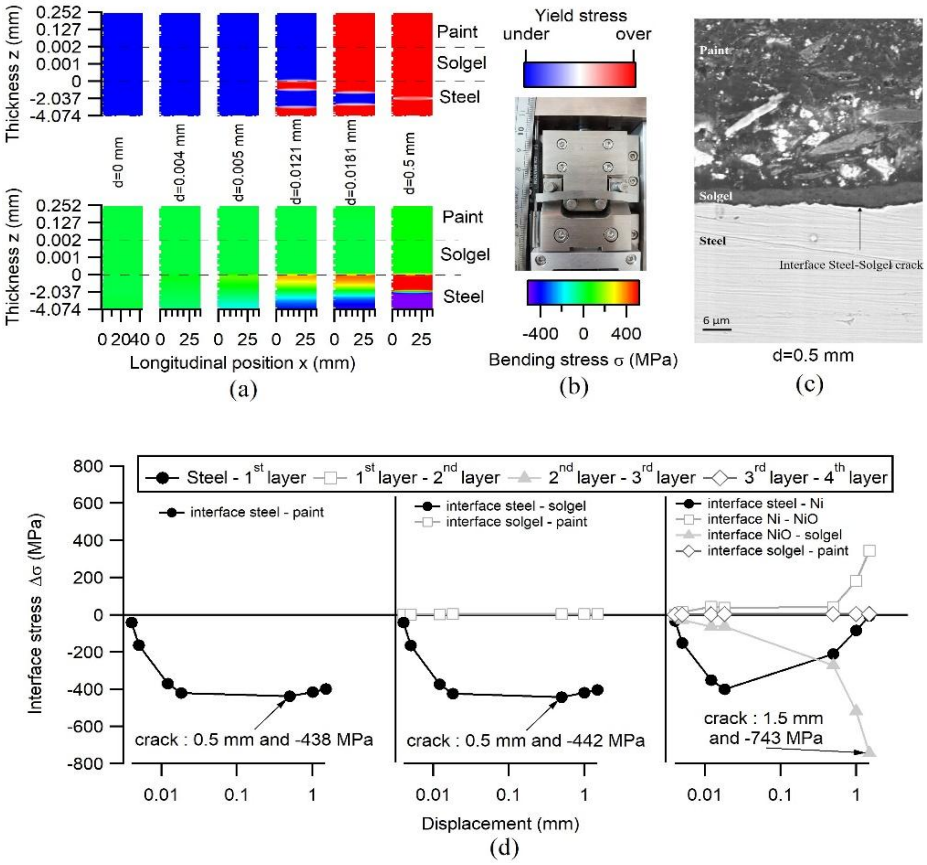

Fig. 3. *In-situ* four-point bending in SEM characterization: stress map for sol-gel paint system (a), experimental device (b), SEM observation of the interface crack (c) and comparison between the three systems to predict the failed interface and characterize their adhesions (d).

Fig. 3 (d) depicts the difference of the calculated stress at each interface as a function of the imposed displacement. This figure reveals that only for the PVD/sol-gel/Paint, steel remains protect with the PVD layers since the interface which is delaminated is NiO/sol-gel for a displacement three times larger than for the two other systems. Concerning these two configurations, failure appears at the interface between steel and the first layer for a displacement of 0.5 mm in agreement with SEM observations. This figure plots numerical results supplied by experimental data and aims at predicting which interface will be broken the earliest under mechanical loadings.

Summary

In this study, a new anticorrosive coating is studied and characterized with an original approach of the adhesion between several layers. The use of a model enables to estimate the induced residual stresses and may be extended to *in-situ* deposition in order to understand the emergence of stresses and the associate kinetics. The complementarity between the model and experimental measurements highlights the power of this tool which can predict the interface failure under mechanical solicitation from curvature measurements.

References

[1] P.A. Sorensen, S. Kiil, K. Dam-Johansen and C.E. Weinell, Anticorrosive: a review, J. Coat. Tech. Res., 6 (2009) 135-176.

[2] G. Stoney, The tension of metallic films deposited by electrolysis, Proc. R. Soc. Lond. A, 82 (2009) 172-175.

[3] L. Le Blanc, E. Campazzi and P. Savigne, Sol for sol-gel process coating of a surface and coating method by sol-gel process using same, Patent EP1885911 B1, (2007).

[4] W.J. van Ooij, D. Zhu, M. Stacy, A. Seth, T. Mugada, J. Gandhi and P. Puomi, Corrosion protection properties of organofunctional silanes – an overview, Tsin. Sc. Tech., 10 (2005) 639-664.

[5] J.H. Osborne, K.Y. Blohowiak, S.R. Taylor, C. Hunter, G. Bierwagon, B. Carlson, D. Bernard and M.S. Donley, Testing and evaluation of nonchromated coating systems for aerospace applications, Prog. Org. Coat., 41 (2001) 217-225.

[6] A.P. Ehiasarian, J.G. Wen an I. Petrov, Interface microstructure engineering by high power impulse magnetron sputtering for the enhancement of adhesion, J. App. Phys., 101 (2007) 1-10.

[7] D.T. Nguyen, A. Ferrec, J. Keraudy, M. Richard-Plouet, A. Goullet, L. Cattin, L. Brohan and P.Y. Jouan, Ellipsometric and XPS characterization of transparent nickel oxide thin films deposited by reactive HiPIMS, Surf. Coat. Tech., 250 (2014) 21–25.

[8] P. Poolcharuansin and J.W. Bradley, Short-and long-term plasma phenomena in a HiPIMS discharge, Plas. Sour. Sc. Tech., 19 (2010) 025010 1-13.

[9] P.A. Dubos, Influence de la température et du trajet de chargement sur les transitions volume/surface des métaux cubiques à faces centrées, PhD th., University of Normandy, (2013).

[10] M. Tatat, Influence de films fonctionnels sur les propriétés élastiques des substrats associés: application au système Ni/NiO, PhD th., ENSMA, (2012).

[11] B. Panicaud, Contraintes de croissance et cinétiques d'oxydation dans des couches d'oxydes thermiques de fer et de nickel ; Etude in-situ pas diffraction des rayons X et modélisation, PhD th., University of La Rochelle, (2004).

[12] A. Dominguez, J. Castaing, Déformation de l'oxyde de nickel monocristallin, Rev. Phys. App., 11 (1976) 387-391.

[13] C. Liu, A.M. Huntz, J.L. Lebrun, Origin and development of residual stresses in the Ni/NiO system: in-situ studies at high temperature by XRD, Mat. Sc. Eng. A, 160 (1993) 113-126.

[14] F. Compoint, Développement de revêtements optiques hybrids organiques-inorganiques pour limiter l'endommagement laser, PhD th., University François Rabelais of Tours, (2015).

[15] G.M. Pharr and W.C. Oliver, Measurement of thin film mechanical properties using nanoindentation, MRS Bull., (1992) 29-33.

[16] X. C. Zhang, B. S. Xu, H. D. Wang and Y. X. Wu, An analytical model for predicting thermal residual stresses in multilayer coating systems, Th. Sol. Fil., 488 (2005) 274-282.

[17] J. Keraudy, Synthèse de couches minces à base de nickel par pulvérisation reactive DC et HiPIMS pour des applications contre la corrosion atmosphérique, PhD th., University of Nantes, (2015).
[18] Q. Hatte, P. Casari, P.Y. Jouan, M. Richard-Plouet, P.A. Dubos, S. Branchu, N. Guitter, R. Coulais, Characterization of corrosion resistant coatings deposited on steel, Poster presentation, EMRS Strasbourg, (2017).